DOI: 10.1002/chem.200500600

Continua of Interactions between Pairs of Atoms in Molecular Crystals

Paulina M. Dominiak,[a] Anna Makal,[a] Paul R. Mallinson,[b] Kinga Trzcinska,[a] Julita Eilmes,[c] Eugeniusz Grech,[d] Maksymilian Chruszcz,[e] Władek Minor,*[e] and Krzysztof Woźniak*[a]

Abstract: The electron density distributions in crystals of five previously studied DMAN complexes and five Schiff bases (two new ones) have been analysed in terms of various properties of bond critical points (BCPs) found in the pair-wise interactions in their lattices. We analysed the continua of interactions including covalent/ionic bonds as well as hydrogen bonds and all other types of weak interactions for all pairs of interacting atoms. The charge density at BCPs and local kinetic and potential energy densities vary exponentially with internuclear distance (or other measures of separation). The parameters of the dependences appear to be characteristics of particular pairs of atom types. The Laplacian and the total (sum of kinetic and potential) energy density at BCPs show similar behaviour with the dependence being of the Morse type. The components λ_1, λ_2, λ_3 of the Laplacian at BCPs vary systematically with internuclear distance according to the type of atom pair. For λ_1 and λ_2 the distribution is of the exponential type, whereas λ_3 does not seem to follow any simple functional form, consistent with previous theoretical findings. Analytical nonlinear dependences of Laplacian on charge density have been found. They agree reasonably well with those obtained by least square fit of the Laplacian to charge density data. There are four distinct regions of the $\nabla^2\rho_{BCP}/\rho_{BCP}$ space, generated by $E_{BCP}=0$ and $G_{BCP}/\rho_{BCP}=1$ conditions. Two regions clearly correspond to the shared-shell and closed-shell interactions and the other two to some intermediate situation.

Keywords: charge density distributions · hydrogen bonds · protonation · Schiff bases · weak interactions

Introduction

Following our previous findings,[1] we have utilized Bader's AIM theory[2,3] to extend the analysis of the continuum of weak interactions to all pairs of interacting atoms found in their crystal lattices, starting from the covalent bonds and finishing with van der Waals contacts, through the whole range of hydrogen bonds, π···π stacking, H···H interactions. The following types of interactions were studied: $[O\cdots H\cdots O]^-$, OH···O, $[N^+H\cdots O^-]$, CH···O, OH···N, $[NH\cdots N]^+$, CH···N, CH···Cπ, Cπ···Nπ, Cπ···Cπ, CH···Cl, H···H, $NO_{nitro}\cdots H$, $NO_{nitro}\cdots C\pi$, $NO_{nitro}\cdots N\pi$, $NO_{nitro}\cdots NO_{nitro}$, O···O, O···Cπ, N-H, O-H, C-H, C-C, C=C, C-O, C=O, C-N, C=N, N=O, $C_{ar}C_{ar}$.

This work also follows up extensive studies by Espinosa et al.[4–9] on the topological and energetic properties of the electron density distributions in hydrogen-bonded systems in which the analysis of 83 published charge density experiments on compounds with X-H···O (X = C, N, O) hydrogen bonds is presented. They found a close fit of the local kinetic and potential energy densities at hydrogen bond critical points to an exponential function for closed-shell interac-

[a] Dr. P. M. Dominiak, A. Makal, K. Trzcinska, Prof. K. Woźniak
Department of Chemistry, University of Warsaw
ul. Pasteura 1, 02-093 Warszawa (Poland)
Fax: (+48) 22-822-2892
E-mail: kwozniak@chem.uw.edu.pl

[b] Dr. P. R. Mallinson
Chemistry Department, University of Glasgow
Glasgow G12 8QQ (UK)

[c] Dr. J. Eilmes
Chemistry Department, The Jagiellonian University
Ingardena 3, 30-060 Kraków (Poland)

[d] Prof. E. Grech
Technical University of Szczecin, ul. Piastów 42
71-065 Szczecin (Poland)

[e] Dr. M. Chruszcz, Prof. W. Minor
Department of Molecular Physiology and Biological Physics
University of Virginia, PO Box 800736
Charlottesville, VA 22908-0736 (USA)
Fax: (+1) 434-982-1616
E-mail: wladek@iwonka.med.virginia.edu

tions.[4] They also found a number of relations between kinetic and potential energy densities and Hessian eigenvalues.[5,6] Espinosa et al.[4–9] showed that the interaction potential derived from the total energy density follows well-defined functional forms, such as Morse, Buckingham, or Matsuoka–Clementi–Yoshimin.[7] In some recent papers based on quantum-mechanical calculations for X-H···F hydrogen bonds, they found a similar functional form for the variation of Laplacian at critical points with H···F distance.[8,9]

Spackman[10] proved that the essential behavior exhibited by multipole-refined electron densities for X-H···O contacts could be described by the superposition of electron densities of O and H atoms. The promolecule, a model of non-interacting overlapping spherical atomic electron densities, contributes the dominant part of the electron density in the intermolecular regions. The values of the electronic kinetic energy densities G_{BCP} are quite successfully reproduced by the promolecule model, however, experimental estimates for potential energy densities at BCP, V_{BCP}, show systematic differences from the prediction of the promolecule model for H···O distances smaller than 2.3 Å.

The role of neutron data in experimental charge density evaluation was previously examined by Espinosa et al.[6] They analysed the topological properties of hydrogen bonding such as amount of electron density, Laplacian of electron density and Hessian values [ρ_{BCP}, $\nabla^2\rho_{BCP}$, and λ_{3BCP}] at the bond critical points with respect to H···CP, CP···acceptor and H···acceptor distances. They concluded that the implicit neutron information introduced by means of average distances observed from neutron experiments was presently good enough to describe the topological properties.

Alkorta et al.[11] found a logarithmic relationship between the bond distances (d_{CH}) in covalent C–H and C···H hydrogen bonds and ρ_{BCP} in their computational studies. They also suggested that a logarithmic relationship between the electron density and the bond length should be found for any A–B pair of atoms.

Abramov[12] proposed a new approach for the evaluation of $G(r)$ and $V(r)$ from experimental (multipole-fitted) electron density. This approach allows a relatively accurate description of the closed-shell medium-range (~1–4 Bohr = 0.53–2.12 Å) behavior of the kinetic energy density. In this approach, the short-range (core region) and long-range values are not well reproduced. The ratio G_{BCP}/ρ_{BCP} should be less than unity and E_{BCP} should be negative for a shared-shell interaction (covalent bond) and this ratio should be greater than unity for a closed-shell interaction (ionic, hydrogen or van der Waals bond). The differences between theoretical values and those obtained from their expressions are about 10% for G_{BCP} and about 20% for V_{BCP} at about 2.2 Å separation. As Abramov[12] pointed out, the biggest contribution to the systematic error in G_{BCP} is expected to be due the $\nabla^2\rho_{BCP}$ term. The $\nabla^2\rho$ displays dependence on $(\sin\theta/\lambda)^2$[13] and is very sensitive to improperly deconvoluted thermal motions.

Finally, Costales et al.[14] presented some general theoretical considerations regarding interactions of pairs of atoms as a function of interatomic separation and stressed the role of the equilibrium distance on main atomic pairs in variety of different bonding regimes.

In the present work, we aim to analyse relationships between parameters of electron density at the bond critical points in the previously studied DMAN[15] and its complexes[1,16,17] and a series of already studied[18] and some new Schiff bases *N*,*N*′-bis(2,5-dihydroxybenzylidene)-1,2-diaminobenzene (**S4**) and tris(3-formyl-5-methyl-2-salicylidenaminoethyl)amine (**S5**, see Figure 1). **S5** forms molecular crystals consisting of two tripodal moieties which form different types of intramolecular hydrogen bonding with O-H···N hydrogen bonds in all three wings of the first moiety and [O^-···H-N^+] hydrogen bonding in the other moiety. Extending our previous findings[1] we want to verify how consistent the charge density data are for so much different classes of compounds as proton sponge complexes and Schiff bases. We also want to include different covalent bonds into our

Abstract in Polish: *Rozkłady gęstości elektronowej w kryształach pięciu uprzednio przebadanych kompleksów DMANu oraz pięciu zasadach Schiffa (w tym dwóch nowych związkach) przeanalizowane zostały w funkcji różnych własności punktów krytycznych wiązań/oddziaływań (BCPs). BCPs charakteryzują oddziaływania między parami atomów w sieciach krystalicznych. Znaleźliśmy continua oddziaływań składające się z oddziaływań kowalencyjnych/jonowych jak również różnych typów wiązań wodorowych oraz innych słabych oddziaływań wszystkich par oddziałujących atomów. Gęstość elektronowa w punktach krytycznych wiązań, lokalna gęstość energii kinetycznej i potencjalnej zmieniają się eksponencjalnie w funkcji odległości międzyatomowej (lub innego parametru charakteryzującego tę odległość). Parametry takich zależności okazują się być charakterystyczne dla poszczególnych par oddziałujących atomów. Laplasjan oraz całkowita lokalna gęstość energii w punktach krytycznych oddziaływań (suma lokalnej gęstości energii kinetycznej oraz potencjalnej) podlegają podobnym zależnościom opisywanym krzywymi typu funkcji Morsa. Składowe Laplasjanu, λ_1, λ_2, λ_3, w punktach krytycznych oddziaływań zmieniają się systematycznie jako funkcja parametru odległości międzyatomowej oraz rodzaju oddziałujących atomów. λ_1 i λ_2, zależą eksponencjalnie od parametru odległości, natomiast λ_3 wydaje się nie podlegać żadnej prostej i znanej zależności. Jest to zgodne z przewidywaniami teoretycznymi. Zostały znalezione analityczne nieliniowe zależności Laplasjanu od ładunku. Są one zgodne z zależnościami uzyskanymi poprzez dopasowanie Laplasjanu metodą najmniejszych kwadratów do danych opisujących gęstości elektronowe w punktach krytycznych. Znalezione zostały cztery obszary w przestrzeni rozpiętej na wartościach laplasjanu i gęstości ($\nabla^2\rho_{BCP}/\rho_{BCP}$) przez warunki $E_{BCP}=0$ oraz $G_{BCP}/\rho_{BCP}=1$. Dwa obszary związane są z oddziaływaniami kowalencyjnymi i jonowymi, natomiast pozostałe dwa nie są jeszcze zbadane i wydają się opisywać sytuacje pośrednie.*

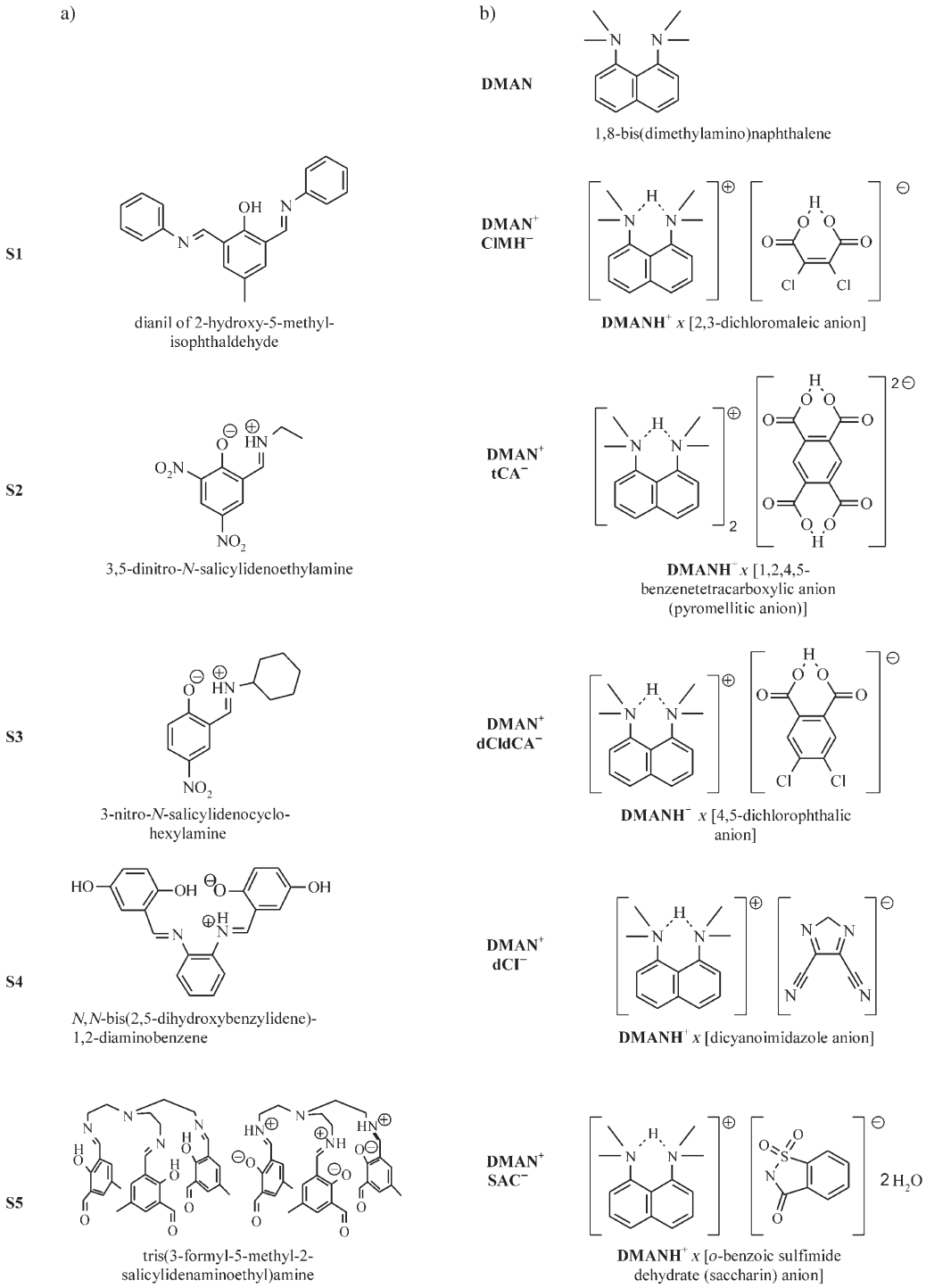

Figure 1. Compounds studied: a) *ortho*-hydroxy Schiff bases, b) DMAN [1,8-bis(dimethylamino)naphthalene] and its ionic complexes. **S5** consists of two tripodal moieties with different types of hydrogen bonding in their molecular fragments.

analysis and a larger range of the weakest interactions (for example H···H interactions and various van der Waals contacts) so as to encompass all bonding interactions present in the crystal lattices. Finally, both ρ_{BCP} and $\nabla^2\rho_{BCP}$ are expressed in terms of a measure of separation. However, we will try to obtain, by elimination of separation parameter from these dependences, the exact functional dependence of $\nabla^2\rho_{BCP}$ on ρ_{BCP} which—in general—should be not linear.

Experimental Section

Experimental electron density measurements: Crystals of the newly obtained Schiff bases studied were orange prisms, grown from acetone/hexane 1:1 (**S4**) and acetonitrile (**S5**). They were obtained by using routine synthetic methods of condensation of aldehydes with appropriate amines.[19]

Single-crystal, high resolution, low temperature X-ray diffraction data for **S4** compound were collected for a single crystal of dimensions 0.35×

$0.30 \times 0.25\ mm^3$ by using the Bruker-Nonius Kappa CCD diffractometer and Oxford Cryosystems low temperature attachment. Data reduction and empirical absorption corrections were carried out with the DENZO[20] and SORTAV.[21]

The **S5** crystal (dimension $0.30 \times 0.30 \times 0.20\ mm^3$) data were collected by using the Rigaku RAPID curved IP system equipped with AFC-9 goniostat and controlled by HKL2000[20] program suite. The high-resolution diffraction experiment was carried out at 103 K using the X-stream Cryogenic Cooler System (Molecular Structure Corporation, Rigaku). The $Mo_{K\alpha}$ X-ray radiation (60 kV, 40 mA) was further monochromatized by graphite monochromator. A total of 960 frames divided into seven omega scans with various χ offsets resulted in a nearly complete data set to 0.46 Å resolution. The exposure time of a single diffraction image was 120 s with 1° oscillation angle. Indexing, integration and scaling were performed with HKL2000. $K\alpha_1$–$K\alpha_2$ split was not taken into account. The space group was determined as $R\bar{3}$. In the merging procedure, the 283394 measured reflections were reduced to 21559 unique reflections. The multi-scan absorption correction was applied in the scaling procedure.[22] The transmission factors T_{min} and T_{max} were 0.985 and 0.897. The refined mosaicity was 0.5° Completeness [%] was equal to 99.6(97.9)*, average redundancy was 13.2(4.7)*.and the average $I/\sigma I$) 43.7(2.6)*, where the data for the highest resolution shell (0.48–0.46 Å) are reported in parenthesis and marked with asterisk.

Multipole refinement: The program XDLSM of the package XD[23] was used for the multipole refinement. The Hansen–Coppens formalism,[24] was applied, the atomic electron density being divided into three components:

$$\rho_k(\mathbf{r}_k) = \rho_{core}(\mathbf{r}_k) + P_{valence}\kappa^3\rho_{valence}(\kappa\mathbf{r}_k) + \kappa'^3 \sum_{l=0}^{l_{max}} R_l(\kappa'\mathbf{r}_k) \sum_{m=-1}^{+l} P_{lm\pm} d_{lm\pm}(\vartheta_k,\varphi_k)$$

a) a spherically averaged free-atom Hartree-Fock core contribution, ρ_{core}; b) a spherically averaged free-atom Hartree-Fock normalized to one electron valence contribution, $\rho_{valence}$, with population parameter $P_{valence}$ and modified by the dimensionless expansion–contraction parameter κ; and c) a deformation term representing the deviation of the valence density from spherical symmetry modified by the dimensionless expansion-contraction parameter κ'. The deformation is expressed in terms of a normalized Slater-type radial function $R_l(\mathbf{r}_k)$ modulated by density normalized, real spherical harmonic angular functions $d_{lm\pm}(\vartheta,\phi)$ defined on local axes centered on the atoms and with population parameters $P_{lm\pm}$. Anisotropic temperature factors were applied to describe the thermal motion of non-hydrogen atoms. Scattering factors for C, H, O and N were derived from wavefunctions tabulated by Clementi and Roetti.[25]

The multipole expansion was truncated at the hexadecapole level for carbon, oxygen and nitrogen atoms, and at the dipole level for hydrogen atoms. Since most of the atoms were in general positions the space group symmetry places no restrictions on the allowed multipole functions. The exceptions are N1 and N3 amine atoms in **S5** structure, for which constraints adequate for threefold axis were applied. Separate κ, κ' were employed for aromatic C, methylene C, N, O, and H. Their values were allowed to vary, except for those relating to H and κ' for O of **S4** which were fixed at theoretically derived values.[26]

CCDC-265417 (**S4**) and -265418 (**S5**) contain the supplementary crystallographic data for this paper. These data can be obtained free of charge from The Cambridge Crystallographic Data Centre via www.ccdc.cam.ac.uk/data_request/cif.

The other numerical data analysed can be found in the Supporting Materials of references [1] and [18].

The data collection and processing statistics are given in Table 1.

Table 1. Crystal data for **S4** and **S5**.

Compound	**S4**	**S5**
formula	$C_{20}H_{16}O_4N_2$	$[C_{33}H_{36}O_6N_4]_2$
F_w	348.36	1169.3
T [K]	100	103
λ [Å]	0.7107	0.7107
crystal system	triclinic	trigonal
space group	$P\bar{1}$	$R\bar{3}$
unit cell dimensions		
a [Å]	8.6760(1)	14.4694(1)
b [Å]	8.9570(1)	14.4694(1)
c [Å]	11.3060(1)	49.5068(4)
α [°]	101.968(1)	90.0
β [°]	108.540(1)	90.0
γ [°]	97.169(1)	120.0
V [Å^3]	797.48(2)	8976.28(4)
Z	2	6
ρ_{calcd} [Mg m^{-3}]	1.451	1.289
$[\sin\theta/\lambda]_{max}$	1.08	1.03
μ [cm^{-1}]	1.0	0.9
$F(000)$	364	3720
index ranges		
	$-18 \le h \le 18$	$-31 \le h \le 31$
	$-19 \le k \le 19$	$-31 \le k \le 31$
	$-24 \le l \le 24$	$-107 \le l \le 107$
no. of data	16428	21482
refls included	12146	17022
R_{int}	0.038	0.028
refinement method		
$[I/\sigma(I)]$ threshold	3	1
N_{ref}/Nv	12.69	14.24
GOFw	2.2788	2.4024
$R\{F\}$	0.0313	0.0363
$R\{F^2\}$	0.0506	0.0250
$R_{all}\{F\}$	0.0627	0.0637
$R_{all}\{F^2\}$	0.0546	0.0267
$R_w\{F\}$	0.0336	0.0176
$R_w\{F^2\}$	0.2244	0.0350
DMSDA(max) [Å^2]	12	19
max(shift/esd)	4×10^{-7}	5×10^{-8}
largest diff. peak and hole [e Å^{-3}]	0.38, −0.36	0.18, −0.21

Results and Discussion

The BCP position: The position of BCP along the bonding path depends on the difference in electronegativities of atoms X and Y. Figure 2 illustrates the relationship between the distance XCP from the atom X to the critical point, and the distance CPY from the critical point to the atom Y. Data points represent any kind of X···Y interaction. They were prepared in such way that XCP is always shorter than or equal to CPY. The sum of XCP and CPY will hereafter be abbreviated as R_{ij}. The graph of CPY versus XCP gives lines with slope −1 and intercept R_{ij}. Each negative diagonal line CPY = −XCP+R_{ij} represents a constant R_{ij} value. The points laying on the XCP = CPY line obviously represent those interactions in which BCPs are equally distant from X and Y atoms.

The covalent bonds to hydrogen atoms (those with R_{ij} ca. 1 Å) keep constant values of R_{ij} because they are constrained to have the average values obtained from neutron diffraction. However, we still observe a systematic variation of

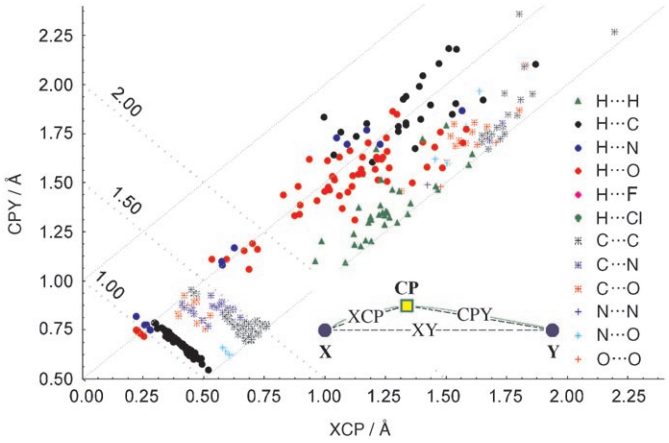

Figure 2. Scatter plot of the XCP and CPY distances for the X···Y atom pair interactions in the crystal lattices of the Schiff bases. The data are ordered in such a way that XCP is less than or equal to CPY.

the CP positions, which allows the electron density to adjust to the constraints imposed. It is particularly well seen for H–C covalent bonds, for which the variation of the CP positions is bigger than in the case of C–C covalent bonds. Systematic variations of BCP position in bonds are observed for computational results obtained for model isolated molecules.[27]

One can not exclude that a similar effect is present for noncovalent H···X interactions in crystals. In general, there is a random distribution of data points for all atom pairs other than X-H. In the case of pairs of the same atom type, most of the points do not lie on the line corresponding to their average R_{ij}. Additionally, there is a spread resulting from variation of CP positions.

***ρ* and Laplacian versus R_{ij}**: It appears that instead of one continuum, as we observed previously,[1] there are separate continua for each pair of interacting atom types. In Figure 3a, we illustrate two classes of such continua for H···X and C···X pairs, where X stands for C, N or O atoms. The separation between the curves depends on the sum of electrons of interacting atoms. The goodness of the fit is insensitive to the definition of internuclear distance (R_{ij}, interatomic distance XY, length of the bonding path BP).

In the case of some better represented interactions such as H···N, H···O, C···C, C···N and C···O, it has been possible to obtain meaningful $\rho_{BCP}(R_{ij})$ dependencies for individual atom pairs. For H···N and H···O atom pairs the differences in the exponent function parameters are significant. It appears that for the shortest R_{ij}, that is, covalent bonds with R_{ij} less than 1.2 Å, the amount of electron density at BCP is larger for H–O than for H–N bonds. The opposite is true for the hydrogen-bond region. In the case of nonhydrogen atom pairs there are no significant differences among the fitted exponential function parameters, however, there is a very significant difference between their exponential coefficients and the ones obtained for the H···N and H···O atom pairs.

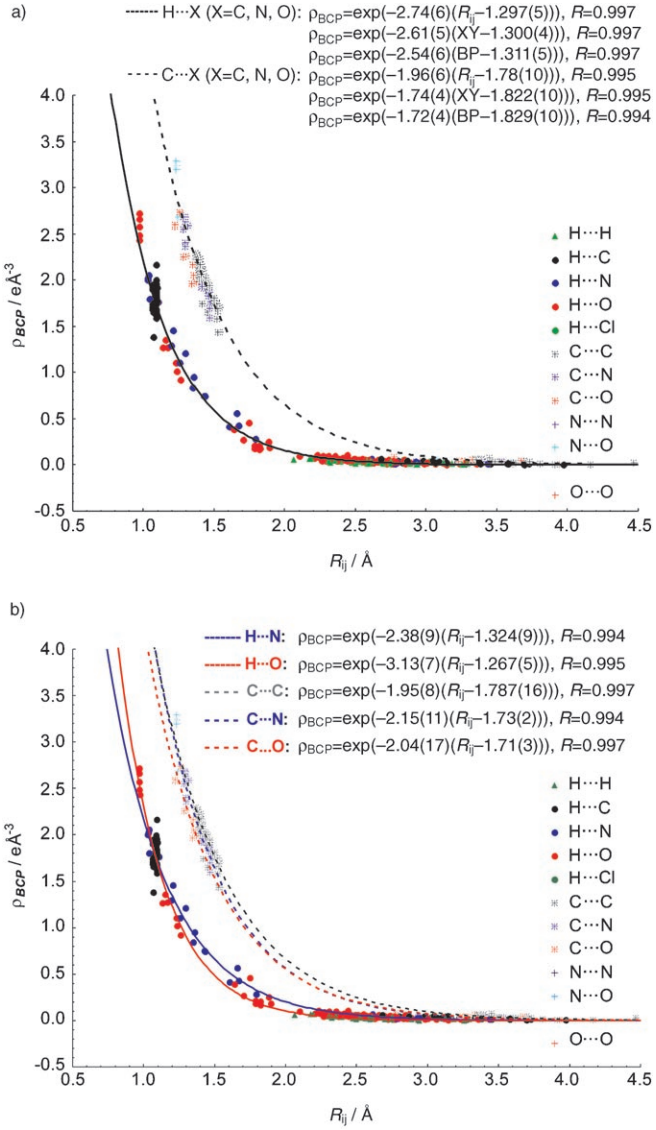

Figure 3. Exponential dependences of ρ_{BCP} on: a) different measures of separation (the sum R_{ij} of the distances from nuclei to the critical point, XY internuclear distance and BP the length of the interaction line) for H···X and C···X pairs of atoms for the Schiff bases and proton sponge complexes; b) R_{ij} for H···N, H···O, C···C, C···N, and C···O pairs of atoms.

The Laplacian values appear to be more sensitive than electron density values at BCPs to type of interacting atoms (Figure 4), as well as to the level of errors associated with experimental procedures and electron density distribution. In this case, we have been able to fit separate Morse curves to the H···O and H···N data. The position of the maximum for the O···H interactions [1.53(3) Å] is shifted towards smaller values compared to the position of maximum for the N···H interactions [1.89(9) Å]. The multiplier of the exponent differs for the two curves and has the values of $-2.46(15)$ Å^{-2} and $-1.6(3)$ Å^{-2} for H···O and H···N, respectively. The lack of experimental data points in the intermediary region of R_{ij} does not allow for interpretation of these differences. For the other atom type pairs, only covalent

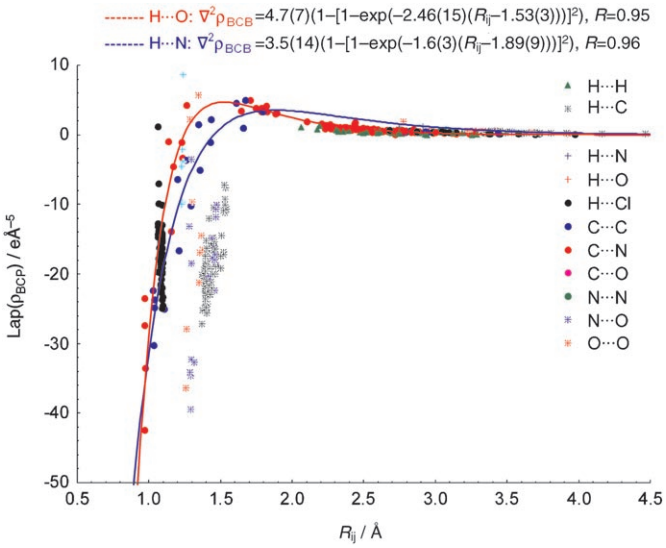

Figure 4. Morse-type dependences of $\nabla^2\rho_{BCP}$ on the sum R_{ij} of the distances from nuclei to the critical point for X···Y pairs of atoms for the Schiff bases and proton sponge complexes.

bonds and very weak interactions are available, therefore we have not fitted any curves to these data.

One can analyse the components λ_1, λ_2 and λ_3 of the Laplacian individually (as shown in Figure 5). The λ_1 and λ_2 distributions fall into two groups as found for the Laplacian itself. Both these distributions take the exponential form compared with the Morse-type dependence of the Laplacian. λ_3 varies in an anomalous fashion in the range R_{ij} from 1.2 to 1.6 Å. The distribution of data points does not follow any simple analytical form. However, it is qualitatively similar to the behaviour of λ_3 found by Espinosa et al.[8] for computed equilibrium structures containing the H···F interactions.

Additionally, there are strong relationships between the local energy densities and the length of the interaction lines (see Figures 6 and 7) again separate for the H···X and C···X, X = C, N, O) classes of interacting atom types. These relationships have similar features as the dependence of ρ_{BCP} on R_{ij}. According to Volkov,[26] the use of his expression for G_{BCP} and V_{BCP} is justified only for the closed-shell medium-range (~1–4 Bohr = 0.53–2.12 Å) interactions. However, in this work we have extended the analysis of the kinetic and potential energy densities to include covalent bonds as well as long range interactions. Although the continua are seen to apply (Figures 6 and 7) to the kinetic and potential energy density distributions throughout the range of R_{ij}, it does not necessarily follow that the energies are estimated correctly in the covalent bond region.

The dependences of the local kinetic and potential energy densities develop the relationships found by Espinosa et al.[2] for energies calculated from topological and structural data for a set of 83 accurate electron density studies involving X-H···O (X = C, N, O) hydrogen bonds. The parameters

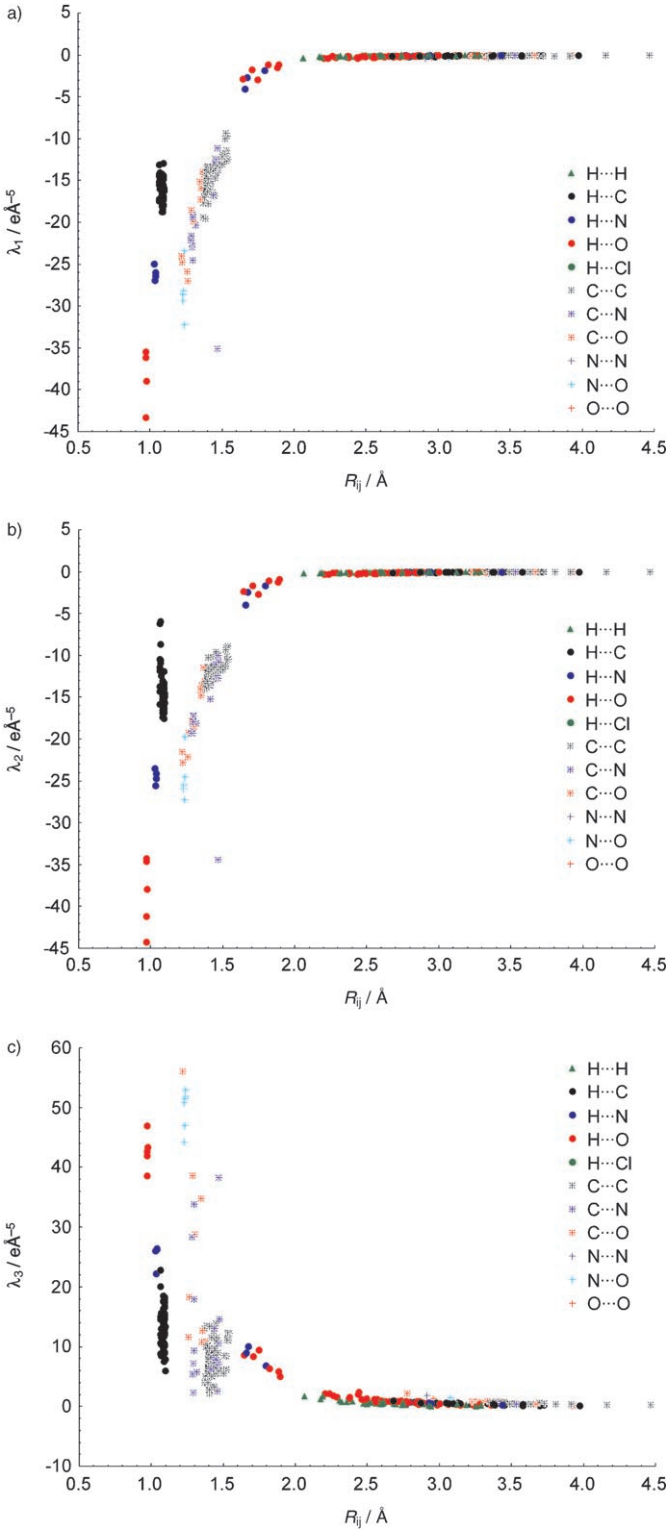

Figure 5. Dependences of the Laplacian components a) λ_1, b) λ_2 and c) λ_3 on the sum R_{ij} of the distances from nuclei to the critical point for X···Y pairs of atoms for the Schiff bases.

of the exponential functions fitted to the data in Figure 5 differ significantly from those found by Espinosa et al. This probably is due to a wider range of types of interactions present in our study.

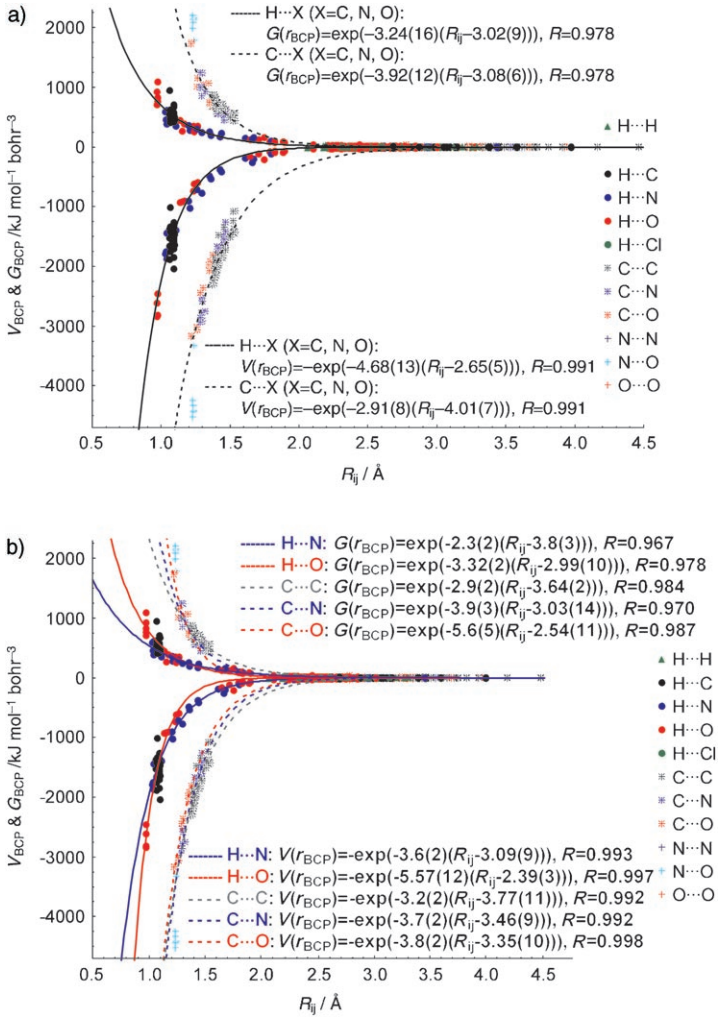

Figure 6. a) Exponential dependences of V_{BCP} and G_{BCP} on the sum R_{ij} of the distances from nuclei to the critical point for X···Y pairs of atoms for the Schiff bases and proton sponge complexes; b) as was the case for $\rho_{BCP}(R_{ij})$ dependence, separate energy curves may be fitted for some individual atom pairs.

For selected pairs of interacting atoms, that is, H···N, H···O, C···C, C···N and C···O, we have been able to obtain individual exponential functions for both local kinetic and potential energy densities. For G_{BCP}, the parameters of the fitted functions show significant differences among the atom pairs. This is not the case for V_{BCP} on R_{ij} dependences. The parameters for potential energy densities are similar for C···C, C···N and C···O interactions, and that stays in agreement with previous observations for the ρ_{BCP} on R_{ij} dependencies.

The total energy density E_{BCP} (Figure 7) describes which type of energy density dominates for a given range of R_{ij}. A positive value signifies that the kinetic energy density dominates and this is the case for the ionic type of interactions. If E_{BCP} is negative the potential energy dominates as is the case for the covalent interactions. The dependence of E_{BCP} on R_{ij} takes the form of the Morse function with a very

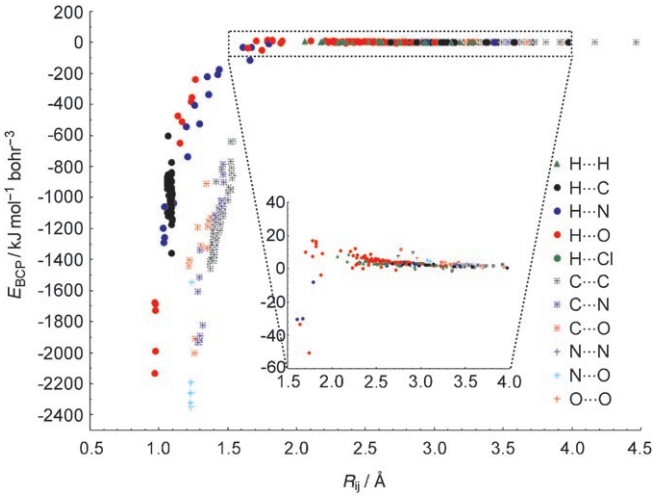

Figure 7. Dependences of the total energy density E_{BCP} on the sum R_{ij} of the distances from nuclei to the critical point for X···Y pairs of atoms for the Schiff bases and proton sponge complexes.

small maximum (ca. 20 kJ mol^{-1} Bohr^{-3} for the H···O pair for example). The region where $E_{BCP} = 0$ corresponds to the boundary between the covalent and ionic interactions.

Usually ρ_{BCP} and $\nabla^2\rho_{BCP}$ are expressed in terms of a measure of separation (Figures 3 and 4), with ρ_{BCP} described as an exponential function of separation:

$$\rho_{BCP}(R_{ij}) = e^{-b(R_{ij}-R_0)}$$

and Laplacian as a Morse-type dependence:

$$\nabla^2\rho_{BCP}(R_{ij}) = d(1-(1-e^{-c(R_{ij}-R_1)})^2)$$

where R_{ij} is a measure of separation, b and R_0 are parameters describing exponential function and d, c and R_1 describe the Morse-type dependence. When the parameter describing separation is eliminated from these dependences, one can obtain the exact functional dependence of $\nabla^2\rho_{BCP}$ on ρ_{BCP} which is not linear (dashed lines in Figure 8):

$$\nabla^2\rho_{BCP}(\rho_{BCP}) = d(1-(1-e^{-c(R_0-R_1)}(\rho_{BCP})^{\frac{c}{b}})^2)$$

This dependence has its maximum (ca. 0.3 e Å^{-3} for the H···N and 0.5 for the H···O interactions) and smoothly goes from the positive to negative values of the Laplacian.

These two variables, $\nabla^2\rho_{BCP}$ and ρ_{BCP}, can also be fitted directly (solid lines in Figure 8). For the H···O data points (red lines), there is a good agreement between the fitted and analytical dependences. For the H···N the correspondence between the two lines is slightly worse, especially in the region of the highest values of ρ_{BCP}. An exception to these fits is apparent in the case of some C=O and all N=O double bonds.

Figure 9 contains the same data as Figure 8 with illustration of two conditions $E_{BCP}=0$ (green dashed line) and $G_{BCP}/\rho_{BCP} = 1$ (red dashed line). These two conditions

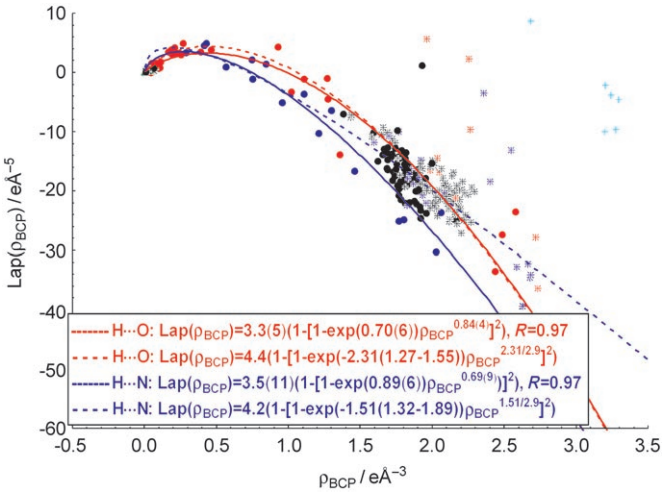

Figure 8. Analytical (-----) and fitted (——) dependences of Laplacian of electron density $\nabla^2\rho_{BCP}$ on the electron density ρ_{BCP} at BCPs for X···Y pairs of atoms for the Schiff bases and proton sponge complexes.

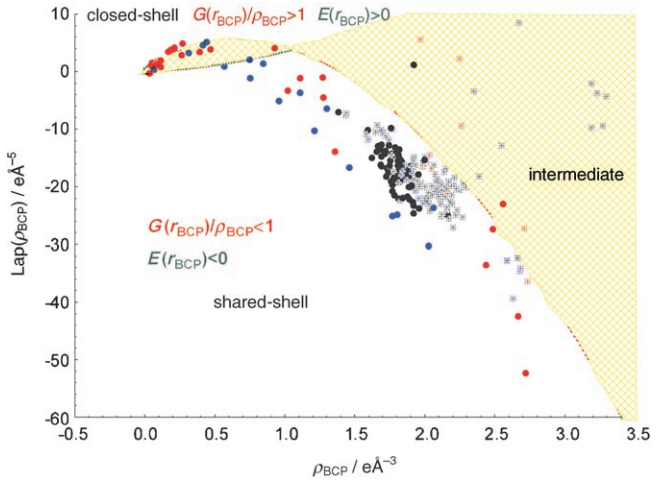

Figure 9. Same data as in Figure 8 with the addition of values for $E_{BCP}=0$ (green) and $G_{BCP}/\rho_{BCP}=1$ (red dashed).

divide the whole area of the plot into four different regions. The first of them ($G_{BCP}/\rho_{BCP}<1$ and $E_{BCP}<0$) corresponds to shared shell interactions. Next, the region with ($G_{BCP}>1$ and $E_{BCP}>0$) corresponds to the closed-shell interactions. The other two regions with ($G_{BCP}<1$ and $E_{BCP}>0$) and ($G_{BCP}>1$ and $E_{BCP}<0$) seem to be intermediary. The question arises whether these regions are equivalent or qualitatively different.

Conclusion

The electron density distributions in crystals of five DMAN complexes and five Schiff bases have been analysed in terms of various properties of BCPs found in the pairwise interactions in their lattices. Despite so significant difference between these two classes of compounds, the charge density data describing both strong and weak interactions allow to find a number of relations between the charge density parameters at BCPs.

CP positions are not, in general, correlated with each other. Even for atom pairs of the same type there is a variation of the internuclear distance. The exceptions are the H–C, H–N and H–O covalent bonds, in which these distances were constraint to their standard values obtained from neutron diffraction and which are, therefore, 100% correlated. Here positions of the CPs vary along the internuclear vectors. So when one is aiming at the highest possible quality of experimental charge densities, the neutron data are highly desirable.

The charge density at BCPs varies exponentially with internuclear distance, this behaviour extending from weak interactions to covalent bonds. The parameters of the dependence appear to be characteristics of particular pairs of atom types. The Laplacian at BCPs shows similar behaviour, the dependence here being of the Morse-type.

The components λ_1, λ_2, λ_3 of the Laplacian at BCPs vary systematically with internuclear distance according to the type of atom pair. For λ_1 and λ_2 the distribution is of the exponential type, whereas λ_3 does not seem to follow any simple functional form, consistent with previous theoretical findings.

Local kinetic and potential energy densities, calculated from the experimental electron density and Laplacian values at BCPs, vary with internuclear distance in an analogous fashion to the charge densities, again depending on the type of atom pair. Furthermore, the parameters of the distribution show some variation from those found for a different set of molecular crystals in other published work. The total (sum of kinetic and potential) energy density varies with the internuclear distance as a Morse function with a very small maximum.

Elimination of the internuclear separation from the fitted dependences on it of charge density and Laplacian, leads to an empirical, nonlinear dependence of Laplacian on charge density. Distinct forms for different atom type pairs necessarily exist as a result of the derivation, and these analytical dependences fairly well match those obtained by direct fitting to the Laplacian versus electron density data. The $\nabla^2\rho_{BCP}/\rho_{BCP}$ space is divided into four distinct regions by two lines, being the conditions $E_{BCP}=0$ and $G_{BCP}=1$. Two of these regions clearly correspond to the shared-shell and closed-shell interactions, the other two to some intermediate situation.

Acknowledgements

P.M.D. and K.W. are grateful for a financial support founded by the Polish State Committee for Scientific Research, KBN, grant 4 T09A 212 25. This work was partially supported by contract GI11496 from HKL Research, Inc. The authors would like to thank the Rigaku/MSC for loaning of the RAPID system.

[1] P. R. Mallinson, G. T. Smith, C. C. Wilson, E. Grech, K. Woźniak, *J. Am. Chem. Soc.* **2003**, *125*, 4259–4270.
[2] R. F. W. Bader, *Atoms in Molecules: A Quantum Theory*, Oxford University Press, Oxford (UK), **1990**.
[3] R. F. W. Bader, *J. Phys. Chem.* **1998**, *A102*, 7314–7323.
[4] E. Espinosa, E. Molins, C. Lecomte, *Chem. Phys. Lett.* **1998**, *285*, 170–173.
[5] E. Espinosa, C. Lecomte, E. Molins, *Chem. Phys. Lett.* **1999**, *300*, 745–748.
[6] E. Espinosa, M. Souhassou, H. Lachekar, C. Lecomte, *Acta Crystallogr. Sect. B* **1999**, *55*, 563–572.
[7] E. Espinosa, E. Molins, *J. Chem. Phys.* **2000**, *113*, 5686–5694.
[8] E. Espinosa, I. Alkorta, I. Rozas, J. Elguero, E. Molins, *Chem. Phys. Lett.* **2001**, *336*, 457–461.
[9] E. Espinosa, I. Alkorta, J. Elguero, E. Molins, *J. Chem. Phys.* **2002**, *117*, 5529–5542.
[10] M. A. Spackman, *Chem. Phys. Lett.* **1999**, *301*, 425–429.
[11] I. Alkorta, I. Rozas, J. Elguero, *Struct. Chem.* **1998**, *9*, 243–245.
[12] Y. A. Abramov, *Acta Crystallogr. Sect. A* **1997**, *53*, 264–272.
[13] R. F. Stewart, *Chem. Phys. Lett.* **1979**, *65*, 335–342; Y. A. Abramov, *Acta Crystallogr. Sect. A* **1997**, *53*, 264–272.
[14] A. Costales, M. A. Blanco, A. M. Pendás, P. Mori-Sánchez, V. Luaña, *J. Phys. Chem. A* **2004**, *108*, 2794–2801.
[15] P. R. Mallinson, K. Woźniak, C. C. Wilson, K. L. McCormack, D. S. Yufit, *J. Am. Chem. Soc.* **1999**, *121*, 4640–4646.
[16] P. R. Mallinson, K. Woźniak, G. T. Smith, K. L. McCormack, *J. Am. Chem. Soc.* **1997**, *119*, 11 502–11 509.
[17] B. Kołodziej, P. M. Dominiak, A. Kościelecka, W. Schilf, E. Grech, K. Woźniak, *J. Mol. Struct.* **2004**, *691*, 133–139.
[18] P. M. Dominiak, E. Grech, G. Barr, S. Teat, P. Mallinson, K. Woźniak, *Chem. Eur. J.* **2003**, *9*, 963–970.
[19] E. H. Charles, L. M. L. Chia, J. Rothery, E. L. Watson, E. J. L. McInnes, R. D. Farley, A. J. Bridgeman, F. E. Mabbs, C. C. Rowlands, M. A. Halcrow, *J. Chem. Soc. Dalton Trans.* **1999**, 2087–2096.
[20] Z. Otwinowski, W. Minor, *Meth. Enzymol.* **1997**, *276*, 307–326.
[21] R. H. Blessing, *J. Appl. Crystallogr.* **1989**, *22*, 396–397; R. H. Blessing, *Acta Crystallogr. Sect. A* **1995**, *51*, 33–38.
[22] Z. Otwinowski, D. Borek, W. Majewski, W. Minor, *Acta Crystallogr. Sect. A* **2003**, *59*, 228–234.
[23] T. Koritsanszky, T. Richter, P. Macchhi, A. Volkov, C. Gatti, S. Howard, P. R. Mallinson, L. Farrugia, Z. Su, N. K. Hansen, XD—*Computer program package for multipole refinement and topological analysis of electron densities from diffraction data*, **2003**.
[24] P. Coppens, X *-Ray Charge Densities and Chemical Bonding*, Oxford University Press, New York, **1997**.
[25] E. Clementi, C. Roetti, *At. Data Nucl. Data Tables* **1974**, *14*, 177–478.
[26] A. Volkov, Y. A. Abramov, P. Coppens, *Acta Crystallogr. Sect. A* **2001**, *57*, 272–282.
[27] S. J. Grabowski, M. A. Walczak, T. M. Krygowski, *Chem. Phys. Lett.* **2004**, *400*, 362–367.

Received: May 29, 2005
Revised: August 18, 2005
Published online: January 3, 2006

